Time and pH Dependence of the L-to-M Transition in the Photocycle of Bacteriorhodopsin and Its Correlation with Proton Release

Thomas Althaus and Manfred Stockburger*

Abteilung Spektroskopie, Max-Planck-Institut für Biophysikalische Chemie, Am Fassberg, D-37077 Göttingen, Germany

Received June 23, 1997; Revised Manuscript Received December 29, 1997

ABSTRACT: The pH dependence of the L-to-M transition in the photocycle of bacteriorhodopsin was studied in pump−probe resonance Raman (RR) flow experiments in the range pH 3.5−7.8 on a time scale of 0−700 μs. For pH < 5, following the initial decay of L to M, the two intermediates approach nearly constant levels. From a specially designed perturbation−relaxation experiment at pH 4.6, in which the composition of L and M is perturbed by photoreversal of M, it could be concluded that the incomplete decay of L is due to an intermediate equilibration between L and M. It was found, by both RR and optical transient spectroscopy, that the maximum level of M (∼500 μs) increases with pH according to a pK_a of 5.6 (150 mM Na^+). Since the proton release from an internal group XH to the extracellular surface is determined by nearly the same pK_a of 5.7 [Zimányi, L., Váró, G., Chang, M., Ni, B., Needleman, R., and Lanyi, J. K. (1992) *Biochemistry 31*, 8535−8543], it is concluded that this increase is controlled by the dissociation of XH. From the analysis of the perturbation−relaxation experiments and the multiexponential rise of M, a kinetic scheme with two sequential L−M equilibria is proposed for the L−M transition. By comparison with the time behavior of proton release [Heberle, J., and Dencher, N. A. (1992) *Proc. Natl. Acad. Sci. U.S.A. 89*, 5996−6000], it is suggested that it is the second equilibrium which is further shifted toward the M state by the dissociation of XH. From the magnitude of this shift, it is concluded that the L−M transition and proton release are not as strongly coupled as is generally assumed. Instead, it is proposed that structural changes during the photocycle are the dominating factors which reduce the pK_a of XH to ≈5.7 so that proton release becomes possible under normal conditions.

The retinal protein bacteriorhodopsin (bR), which is found in the archaeon *Halobacterium salinarium*, acts as a light-driven proton pump (for reviews, see refs *1*−*4*). The bR protein molecules are regularly arranged in particular fragments of the cell membrane (purple membrane). On illumination, bR is able to pump protons from the cytoplasmic to the extracellular side of the membrane. This leads to a proton gradient which is used by the cell to drive ATP synthesis. The proton transport across the membrane is linked to a light-induced cyclic reaction (photocycle) of the retinylidene Schiff base chromophore of bR. In the unphotolyzed state, the chromophore has its absorption maximum at ∼570 nm (the parent chromophore is designated by BR_{570}, or simply by BR). After the primary photoreaction in which retinal, in <1 ps, is converted from the *all-trans* to the *13-cis* configuration (ref 5 and citations therein), the chromophore runs through a series of thermally controlled intermediate states

$$K_{590}(5\text{ ps}),\ L_{550}(1.25\ \mu\text{s}),\ M_{412}(100\ \mu\text{s}),\ N_{560}(2-3\text{ ms}),\ O_{640}(3\text{ ms}),\ BR_{570}(10\text{ ms})$$

until the parent-state BR_{570} is reestablished. In this series, the appearance times, given in parentheses, refer to normal conditions (20 °C, neutral pH) and the subscripts denote the absorption maxima in nanometers.

It is well established that during the L−M transition the Schiff base proton is transferred to the counterion D85 (*6*, *7*) and later, during the formation of the intermediate N, is reprotonated. In the past few years, great efforts were made to obtain a deeper insight into the molecular mechanism of proton release to the extracellular surface during the photocycle of bR. Important progress was made when the appearance of released protons could be monitored by pH indicator dyes which were covalently bound to residues at the surface (*8*−*11*). It was found that under normal conditions in wild-type bR the appearance time nearly coincides with the time constant of the L−M transition, i.e., the transfer of the Schiff base proton to the counterion D85 (∼100 μs). However, it was found that the two events do not occur completely synchronously. Since the counterion D85 remains protonated at least throughout the lifetime of M (2−4 ms) it is obvious that the proton which appears on a time scale of ∼100 μs at the extracellular surface is not identical with the original Schiff base proton. It was therefore proposed that the proton release to the surface is mediated by an additional group (*12*). Direct evidence for the existence and function of such a group, called XH, could be inferred from time-resolved titration experiments in which the released protons were monitored by pH indicator dyes in the bulk aqueous medium (*13*). It was found that the release of protons is correlated with a dissociation equilib-

* To whom correspondence should be addressed.

S0006-2960(97)01496-7 CCC: $15.00
Published on Web 02/12/1998

rium between XH and the aqueous medium, which is established during the first phase of the photocycle. For the dissociation of XH, a pK_a of ~5.7 was obtained (in 100 mM KCl) (*13*). This result implicates that "normal" proton translocation (release precedes reuptake) takes place for pH > pK_a = 5.7. It must be noted that for pH < pK_a, the release is delayed until the reuptake of a proton (*13*−*16*). This is also the case in some mutants of bR (ref *17* and citations therein). Evidently the pK_a of XH must be high enough in the unphotolyzed state to prevent its dissociation under normal conditions. XH therefore must be a group close to the surface whose pK_a is drastically reduced during the cycle so that under normal conditions the ejection of a proton becomes possible.

From calculations of pK changes on the time scale of the L−M transition, it was predicted that the residue E204 might be a candidate for XH (*18*−*20*). Indeed, it could be confirmed that this residue must be involved in the release process since in the mutant E204Q the normal release process is abolished (*21*). However, in a recent report, it could be shown that the replacement of the residue E194, which is located close to the extracellular surface, by the residue C194 also inhibits the normal release process (*22*). This suggests that XH is not a single residue but has a more extended structure with contributions from several residues and probably from water molecules. It may also be that the proton is delocalized within this complex. This should be kept in mind when the term "release group" is used.

The results of titration experiments on D85 in the unphotolyzed state of bR play an important role in the present discussion of the release process. Such experiments revealed a strong coupling between D85 and another dissociable group called X′H, in such a way that the pK_a of X′H is drastically reduced by ~5 pH units when D85 is protonated, and conversely, the pK_a of D85 is increased by ~5 pH units once X′H becomes deprotonated (*23*−*25*). It has been argued that X′H is identical with the release group XH (*17*, *22*, *23*, *26*).

It was proposed that the strong coupling between D85 and XH also holds during the photocycle (*17*, *23*). This leads to a model in which the drop of the pK_a of XH from ~9.5 in the unphotolyzed state to ~5.7 during the cycle is induced by the protonation of D85 during the L−M transition (*17*, *23*, *27*). This model supports the general assumption that the L−M transition triggers the release function. However, it must be noted that, due to structural changes during the photocycle, the coupling strength between D85 and XH in the M state may be different from that in the unphotolyzed state. Consequently, it cannot be taken a priori for granted that this coupling is the dominating factor that controls proton release.

From the coupling between D85 and the release group one would expect that under conditions where XH is dissociated (pH >5.7) the often invoked equilibrium between L and M (*1*, *4*) is shifted toward the M state so that the maximum amplitude of M is raised. Indeed, such an effect had been found for wild-type bR and described by a pK_a of 5.6 (*28*). In the case of the recombinant D96N, a corresponding effect, i.e., a decrease of the ratio L/M_{max}, had been reported which is correlated with a pK_a of 5.8 (*13*).

It is thus apparent that the dissociation of XH during the photocycle and consequently the proton release in its pH and time dependence are directly reflected by the L−M transition. To use this correlation as a probe for the release process, we studied the L−M transition in the pH range 3.5−7.8, using both time-resolved resonance Raman (RR) and optical transient spectroscopy.

In the analysis of the photocycle of bR, it is usual to fit the kinetic results by introducing back reactions between two subsequent intermediates *(1, 4)*. This procedure, which is justified for principle reasons, leads to the establishment of intermediate equilibria. In the case of the L−M transition, such an equilibrium is indicated by the observation that for pH <5 the decay of L to M is not complete during the photocycle *(28)*. However, conclusions on the L−M equilibrium, on the basis of kinetic data alone, are ambiguous, since the same time behavior for L and M can be obtained by different kinetic schemes *(28)*. We therefore have designed a special perturbation−relaxation experiment which is based on time-resolved RR spectroscopy. This enabled us to identify the reversibility of the L−M transition in a direct way.

From our data on the time and pH dependence of the L−M transition, a kinetic scheme will be proposed which involves two sequential L−M equilibria. It will be seen that the appearance of the release process shifts the second L−M equilibrium further toward the M state. It is a fundamental question as to whether proton release is triggered by the L−M transition. Mainly due to the near coincidence of the two events, it is widely accepted that this is the case although unequivocal physical evidence is missing. In this paper, this problem is again discussed on the basis of the kinetic data that are presently available. It will be seen that a kinetic scheme in which the two events are not strongly coupled is supported by our results.

MATERIALS AND METHODS

Purple Membranes (PM). These were isolated from *H. salinarium* as described (*29*). Purified samples of PM were provided by the Max Planck Institute for Biochemistry in Munich. All experiments were performed at room temperature (~22 °C) with highly diluted aqueous suspensions of PM, set to an optical density of 1 at 570 nm (16 μM bR). The pH in the PM suspensions was varied between 3.5 and 7.8 by using a 100 mM citrate or phosphate buffer system. The mean concentration of Na^+ was 150 mM (pH 6).

CW Dual-Beam (Pump−Probe) Flow Experiments Using RR Detection. This technique has been described earlier in detail (*28*, *30*). The variable parameters of the pump beam are the rate constant of photolysis (l_0) and the residence time, Δt, of a sample element in the CW laser beam. l_0 is given by the product of the quantum yield of photolysis, the absorption cross section, and the photon flux density of the laser. The residence time Δt is determined by the $1/e^2$ diameter (d_{1/e^2}) of the laser beam and by the flow velocity. The degree of photolysis is determined by the product $l_0\Delta t$ (photoconversion parameter). For sufficient photolysis in the pump beam $l_0\Delta t \geq 1$ is required, whereas in the RR probe beam $l_0\Delta t \ll 1$ is chosen to keep unwanted photolysis at a low level. The delay time, δ, between the photolysis and RR probe events is given by the lateral distance of the two parallel beams and the flow velocity. Normally δ is varied by changing the lateral distance.

As flow system, a spinning cell of cylindrical shape with a diameter of 40 mm and an optical path length of 5 mm was used. The rotational period of the cell was large compared to the period of the photocycle so that unphotolyzed sample always entered the pump beam. The optical layout of the pump−probe experiment, the RR detection equipment, and the analysis of the pump−probe spectra were essentially the same as described in our earlier work (*28*, *30*). A three-beam experiment that consists of two pump beams and a Raman probe beam was designed for the exploration of a potential L−M equilibrium and is described in the text.

Laser Flash Photolysis. Optical transients of purple membrane suspensions were measured at selected probe wavelengths using the same procedure and equipment as described earlier (*28*). However, the energy of a single laser pulse (532 nm, 8 ns) was attenuated by a factor of 3 to ∼1 mJ giving a photoconversion parameter of ∼1. Under such conditions, secondary photoreactions that induce an unwanted long-lived M component can be widely neglected (*31*). To measure the pH dependence of the amplitude of a transient signal in a quantitative way, the following procedure was used: Two samples of different pH but of exactly the same optical density (∼1 at 570 nm) were prepared. One of the samples served as a standard of constant pH. For subsequent pulses of the pump laser (repetition rate 1 s^{-1}), the two samples were moved alternatively into the measuring position where pump and probe beams cross each other under 90°. Since fluctuations between subsequent pulses were small, a quantitative analysis of the two transients at sufficiently high accuracy is possible.

RESULTS

Diagnostic RR Bands in the Photocycle. The temporal evolutions of BR and its intermediates L, M, and N were monitored in pump-and-probe flow experiments as described in Methods (for a recent review, see ref *30*). Since the RR spectrum of BR, and the spectra of L or N strongly overlap under all excitation conditions, the contribution of bR has to be subtracted in order to obtain the pure spectra of L and N. In the case of M, a pure spectrum can be obtained by selective excitation in the violet.

The strongest bands in the RR spectra of the four species of interest are depicted in Figure 1. These bands refer to C═C stretching vibrations of the retinal chain. They differ in a characteristic way, in both frequency and shape, and therefore are ideally suitable for diagnostic purposes. Evidently, the integrated intensities of such bands are directly proportional to the respective concentrations. For a quantitative analysis, the RR cross sections, which for each species correlate intensities and concentrations as a function of excitation wavelength, must be taken into account (*28*). In this paper, we are interested in following the time dependencies of BR, L, M, and N. This can be done in an optimum way by choosing the laser line at 476 nm for excitation since for this line the RR cross sections of the four species are of comparable magnitude. For the analysis of the strongly overlapping RR bands of L and N in the presence of a high population of M, the laser line at 514 nm was used since for this line the RR cross section of M is considerably smaller than that of L or N.

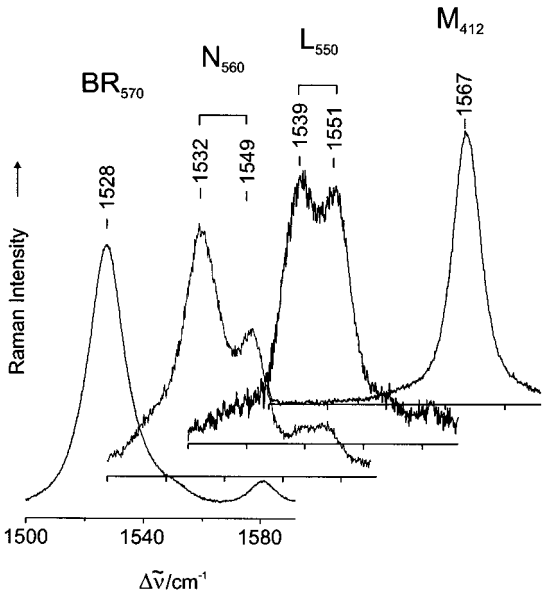

FIGURE 1: The strongest ("diagnostic") bands in the RR spectra of the parent chromophore BR_{570} and the intermediate states L_{550}, N_{560}, and M_{412}. The spectra of the intermediates were obtained in pump−probe flow experiments as described in the text and under conditions where the respective species is significantly accumulated.

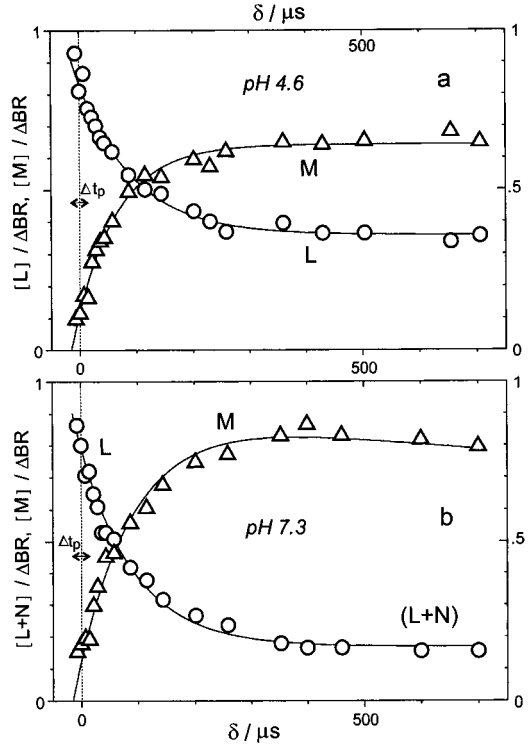

FIGURE 2: Temporal evolution of L, M, and L + N for pH 4.6 and 7.3 on a time scale of 700 μs as deduced from the integrated intensities of the diagnostic RR bands in pump−probe flow experiments. The data are displayed as fractional concentrations normalized to the fraction ΔBR which is photolyzed in the pump beam. Δt_p is the dwell time of a flowing sample element in the pump beam.

The L−M Transition at pH 4.6 and 7.3. The decay of L and the concomitant rise of M, as obtained from RR experiments, are depicted in Figure 2 for pH 4.6 and 7.3 on a time scale of 700 μs. For this diagram, the data from earlier experiments (*28*, *32*) and from our present studies were considered. In all cases, the laser line at 476 nm has been

used for RR excitation. The data are represented as fractional concentrations [BR], [L], [M], and [N] which are defined by

$$f_L I_L + f_M I_M + f_N I_N + I_{BR} = [L] + [M] + [N] + [bR] = 1 \quad (1)$$

where I_L, I_M, and I_{bR} are the integrated RR intensities of the diagnostic bands normalized to the band intensity $I_{BR}(o)$ of unphotolyzed bR. The data were referred to ΔBR, which is the fraction photolyzed in the pump beam. In eq 1, the formation of the intermediate O is neglected, which is justified for the time range under consideration. The factors f_L, f_M, and f_N refer to the ratios of the RR scattering cross section of BR to the respective cross sections of L, M, and N. For $\lambda_R = 476$ nm, the data are consistent with $f_L = 0.82$ and $f_M = 1.6$. For pH 7.3, a conversion of L to N is observed. For instance, at $\delta = 500$ μs, about half of L is transformed to N (*28*). In the analysis of Figure 2, it is assumed that the cross sections of L and N are the same($f_L = f_N$). In view of the great similarity of the two chromophores, this approximation is justified. It can be seen in Figure 2 that for pH 4.6 only ~60% of L is transformed to M. This is entirely different for pH 7.3, where nearly 90% is converted to M or N.

Titration of the L−M Transition. When the pH dependencies of [M] and [L + N] as obtained from earlier data (*28*), monitored for $\delta = 500$ μs, are displayed in the range pH 3.5−7.6 it can be seen that [M] rises at the expense of [L + N] with increasing pH. If the data are fitted by Henderson−Hasselbalch equations ($n = 1$), one obtains pK_a values of ~6.

In the present study the pH-dependent increase of M was tested by two independent measurements. The first one was an RR experiment using a rotating cell with two compartments of equal size which were filled with samples of different pH but of the same optical density. This technique allows one to record the RR spectra of two samples quasi-simultaneously and thus to achieve high accuracy in their comparison (*33*). A specific result is shown in Figure 3a for a pair of samples with pH values of 4.7 and 7.4, respectively. It can be concluded from the analysis of the two bands by a band-fitting procedure that the band maximum of M, probed for $\delta = 430$ μs, increases by a factor of ~1.38 when the pH is raised from 4.7 to 7.4.

The second measurement was based on transient studies at 430 and 412 nm, in the region of the optical absorption band of M. It is evident that the pH-dependent increase of M, as inferred from our RR experiments, should also be observable in optical transient studies. However, such an increase had not been reported earlier for wild-type bR and only had been found for some mutants (*13*, *34*). It was therefore a challenge for us to search for such effects in wild-type bR. For this purpose we designed an experiment that allowed us to determine the amplitude of the transient signal of M as a function of pH in a quantitative manner (see Materials and Methods).

Transients for two different pH values are shown in Figure 3b, confirming the expected increase of the M amplitude. In the representation of Figure 4a, each transient for pH_x is referred to its standard sample at pH 5.1. The amplitudes of the M signals were obtained by fitting the transients with three time constants, one for the rise and two for the decay

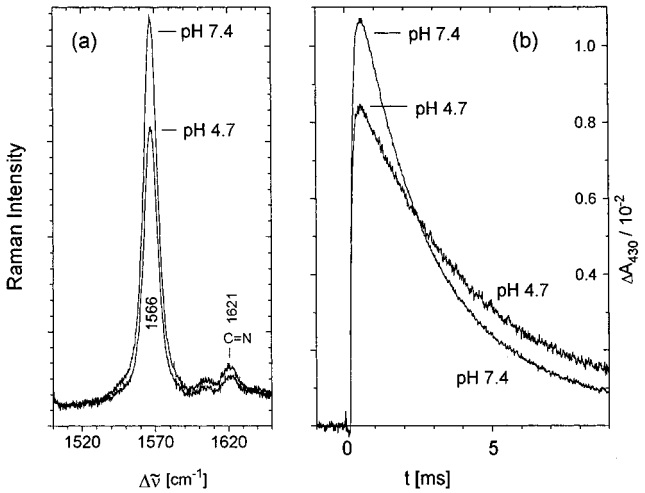

FIGURE 3: (a) The diagnostic RR bands of M probed for $\delta = 430$ μs in pump−probe flow experiments for pH 4.7 and 7.4. A spinning cell was used consisting of two compartments of equal size, filled with samples of different pH but of the same optical density. The band intensities are directly related to the relative concentrations of M in the two samples. Pump beam: $\lambda = 514$ nm (140 mW), $d_{1/e^2} = 100$ μm. Raman probe beam: $\lambda = 406$ nm (9 mW), $d_{1/e^2} = 100$ μm. (b) Optical transient signals, probed at 430 nm for pH 4.7 and 7.4, respectively, using the special measuring procedure described in the text.

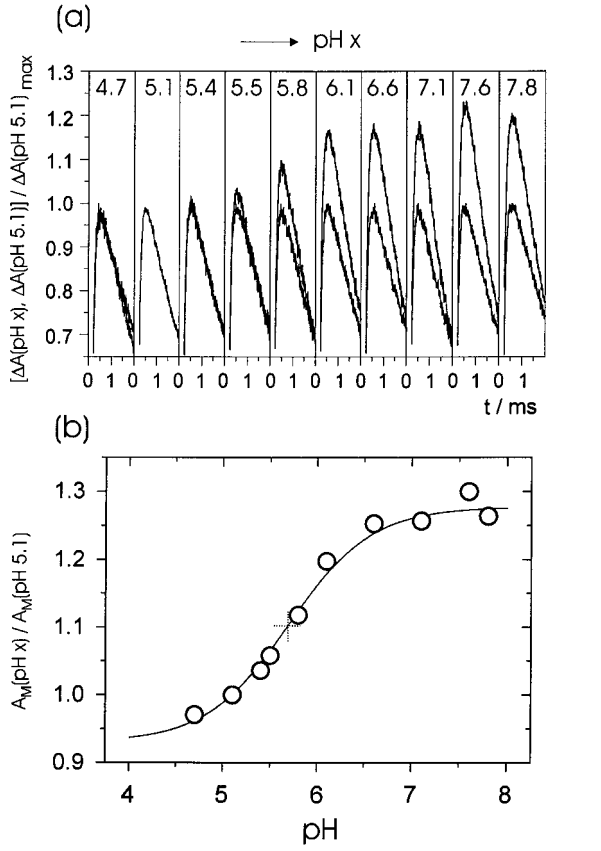

FIGURE 4: (a) Pairs of optical transient signals, obtained as in Figure 3b, in the range pH 4.7−7.8. One of the signals refers to the standard sample at pH 5.1. (b) Normalized amplitudes of M as inferred from the transient signals in (a). The data points are fitted by a Hendersson−Hasselbalch equation with p$K_a = 5.7 \pm 0.1$.

of M. The application of two time constants, for the rise of M (cf. Figure 8) did not change the results. In Figure 4b, the amplitudes obtained in this way for a probe wavelength

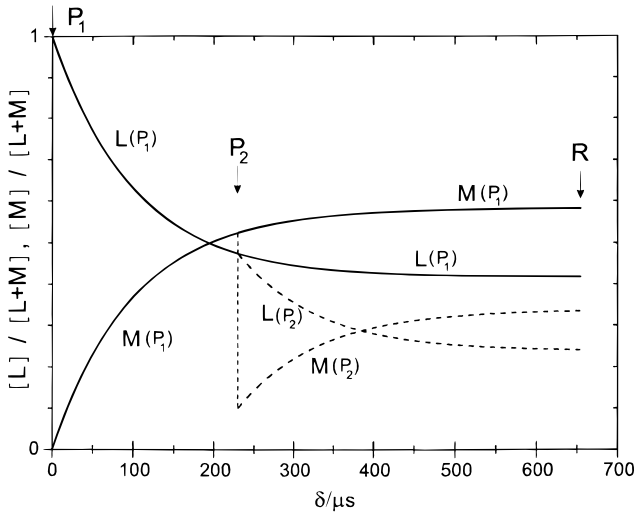

FIGURE 5: Scheme of a three-beam perturbation−relaxation experiment which allows us to examine the existence of an intermediate equilibrium between L and M. P_1: first pump beam which produces $L(P_1)$ and $M(P_1)$ which equilibrate with an arbitrarily chosen time constant of 90 μs. P_2: perturbation beam which depletes $M(P_1)$. R: Raman probe beam by which the composition of L and M can be monitored for different delay times δ. $L(P_2)$ and $M(P_2)$ show the exponential time course of the relaxation event, calculated again for a time constant of 90 μs.

of 430 nm and normalized to the standard sample, are displayed as a function of pH. A fit with a Henderson−Hasselbalch equation ($n = 1$) gives p$K_a = 5.7 \pm 0.1$ and an increase of M from the low- to the high-pH limit by a factor of 1.37 ± 0.04. The experiment was repeated with a probe wavelength of 412 nm giving a pK_a of 5.5 ± 0.123 and an increase by a factor of 1.44 ± 0.08. By averaging such data, one obtains p$K_a = 5.6 \pm 0.1$ and a value of 1.41 ± 0.06 for the increase factor of M.

A Three-Beam Perturbation RR Experiment at pH 4.6. Our results on the time and pH dependence of the L−M transition in the range pH 3.5−7.8 would fit into the following model: In the low-pH limit, an intermediate equilibrium is established between L and M which in the high-pH limit is shifted considerably toward M. The pH transition between the two limits can be described by a pK_a of 5.6. However, this model is ambiguous, since the observed phenomena may be explained in different ways, for instance, by the superposition of different reaction pathways (*28*).

The question of whether and to what extent an L−M equilibrium exists in the low-pH limit can be answered by a perturbation−relaxation experiment as described schematically in Figure 5. A similar experiment had been performed earlier in our laboratory for pH 7 (*35*). In this procedure, the parent chromophore BR_{570} is photolyzed by a first pump beam (P_1) producing $L(P_1)$ and $M(P_1)$. After a delay of 230 μs, the sample is perturbed by a second photolysis beam P_2 which partially reconverts M to BR (*36*−*39*). As a consequence, the fraction of M is significantly reduced. If, as is assumed in Figure 5, L and M undergo an equilibration with a single time constant of ~90 μs, $L(P_2)$ and $M(P_2)$ would relax to the equilibrium after the perturbation event according to this time constant. If, for instance, the sample is probed for $\delta = 655$ μs by the Raman excitation beam R, one would expect that the equilibrium is completely reestablished.

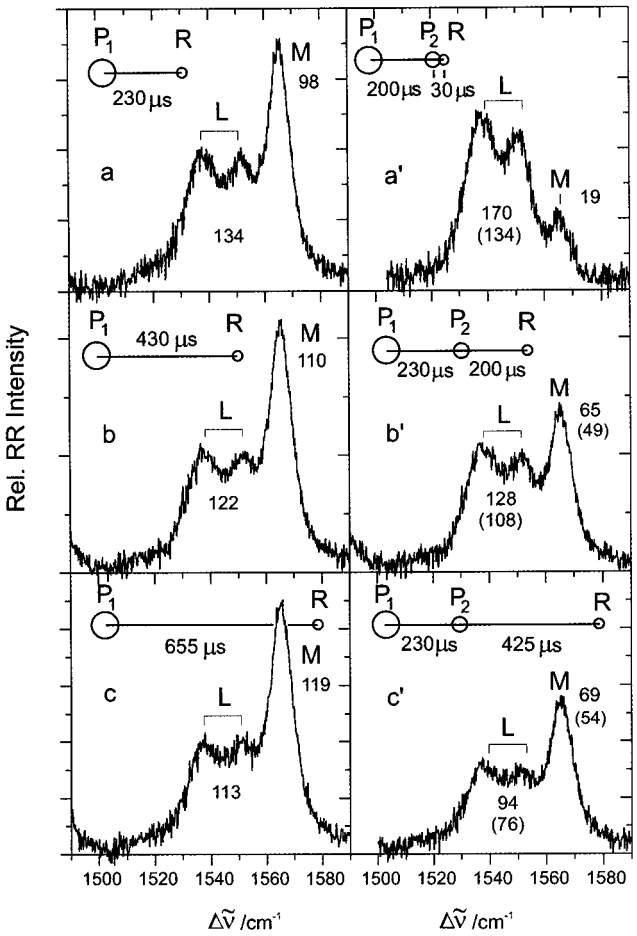

FIGURE 6: Results of a three-beam perturbation experiment for different positions of the two pump beams P_1 and P_2 and the Raman probe beam R. The given numbers refer to the integrated band intensities of the diagnostic RR bands on a relative scale. The numbers in parentheses refer to the corrected intensities as described in the text. The given delay times among P_1, P_2, and R were obtained from the lateral distances of the parallel beams and the flow velocity of the sample in a spinning cell. P_1: $\lambda = 476$ nm (190 mW), $d_{1/e^2} = 220$ μm. P_2: $\lambda = 406$ nm (38 mW), $d_{1/e^2} = 130$ μm. R: $\lambda = 476$ nm (4 mW), $d_{1/e^2} = 80$ μm. Flow velocity, 6 ms^{-1}.

The results of our perturbation−relaxation experiment are displayed in Figure 6. In this representation, the contributions of bR are subtracted. The unmodified spectra have recently been published elsewhere (*30*, *40*). The three parallel CW laser beams P_1, P_2, and R were focused under different diameters into the liquid sample in a rotating cell. Whereas P_1 and R were derived from the same argon ion laser beam at 476 nm, the perturbation beam P_2 at 406 nm was obtained from a krypton laser. All three beams were polarized in the plane of incidence of the spectrometer. As usual, RR scattering was detected perpendicular to the Raman probe beam.

It is an important feature of this experiment that, under otherwise unchanged conditions, the perturbation beam P_2 is interrupted periodically. This allows a quasi-simultaneous recording of the spectra in the presence and absence of P_2. This implies that the spectra in (a, a′), (b, b′), and (c, c′) of Figure 6 refer to exactly the same intensity scale and therefore are directly comparable.

Analysis of the Three-Beam Experiment. The spectra in Figure 6 were analyzed by band-fitting procedures. The

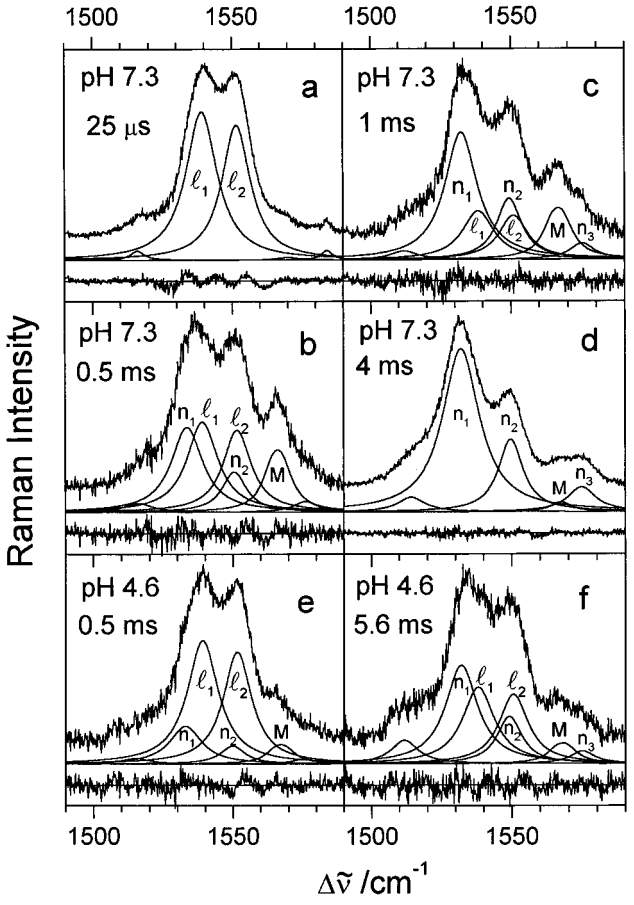

FIGURE 7: Deconvolution of mixed spectra of L, N, and M by band fitting with Lorentzian line shapes on the basis of the pure spectra of L, N, and M. The calculated bands are superimposed on a baseline which for convenience is somewhat downshifted with respect to the true baseline. The difference between the measured and the calculated spectra is given on a second arbitrarily downshifted baseline. (a) Pure L: (position, width, and relative maximum intensitiy of the subbands, respectively): (l_1) 1539 cm^{-1}, 13.7 cm^{-1}, 100 ru; (l_2) 1551.5 cm^{-1}, 12.4 cm^{-1}, 91 ru. (d) Pure N: (n_1) 1532 cm^{-1}, 13.9 cm^{-1}, 100 ru; (n_2) 1549 cm^{-1}, 10.7 cm^{-1}, 48 ru; (n_3) 1575 cm^{-1}, 10.5 cm^{-1}, 13 ru. The pure spectrum of M (cf. Figure 1) consists of two closely lying subbands: (m_1) 1564 cm^{-1}, 8.3 cm^{-1}, 57 ru; (m_2) 1568.4 cm^{-1}, 9.8 cm^{-1}, 100 ru. For the mixed spectra in the following the relative weighting factors are given: (b) L, 100; N, 77; M, 29.4. (c) L, 46.5; N, 100; M, 21. (e) L, 100; N, 25; M, 6.7. (f) L, 95; N, 100; M, 10.8. Pump and probe conditions: (a) pump beam, $\lambda = 647$ nm; Raman probe beam, 514 nm; (b−f) pump and Raman probe beam, 514 nm. In all cases, the general conditions as described in Materials and Methods were applied.

numbers given for the diagnostic RR bands refer to the respective integrated band intensities on the same scale in arbitrary intensity units (iu). A comparison of (a) and (a′) reveals that the intensity of M is reduced by a factor of 5 when P_2 is switched on. Such a high efficiency of the back reaction from M to BR is only obtained for parallel polarization of P_1 and P_2 as was used in our experiment. This back reaction can be directly concluded from an intensity increase of BR in the unmodified spectra (*30*, *40*). A second much smaller effect, induced by P_2, is the increase of L from 134 iu in (a) to 170 iu in (b). This is due to the P_2-induced forward reaction of that fraction of BR (∼60%) which is not photolyzed by P_1. For quantitative considerations corrections have to be made for this effect to the spectra in (a′), (b′), and (c′). In the case of (a′), the correction

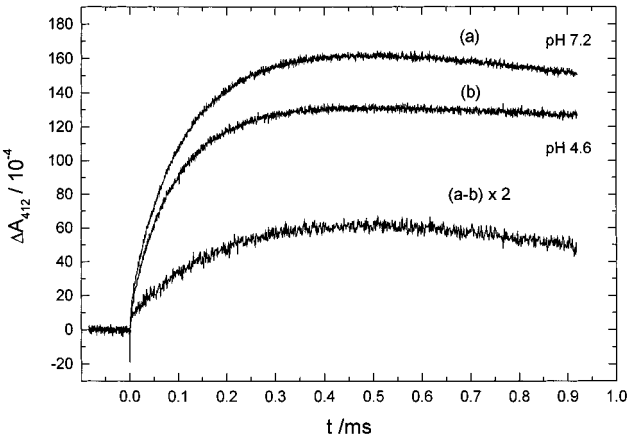

FIGURE 8: Optical transients at 412 nm which display the rise of M for pH 4.6 and 7.2, respectively.

is straightforward, since the P_2-induced increment in L of 170−134 = 36 iu has not yet further developed. In the case of (b′) and (c′), this increment has to be distributed according to the intensity ratio of L and M in (a) and (b). In this way, one obtains the corrected intensities which for (a′), (b′), and (c′) are given in parentheses.

It can be concluded from the corrected intensity values in (b′) and (c′) that after the perturbation event M gradually increases at the expense of L, indicating the reestablishment of the equilibrium value. From such data, a time constant for relaxation to the equilibrium (τ_{rel}) can be obtained. For this purpose, an expression for the ratio [M(P_2)/L(P_2)] is deduced from the relaxation model in Figure 5. This expression depends on τ_{rel}, the delay time δ(P_2,R), and the equilibrium value $[M/L]_{eq}$. In this way, τ_{rel} can be calculated from our data if one takes into account that the concentration ratios [M/L] are obtained by multiplying the respective intensity ratios I_M/I_L by the factor $(f_M/f_L)_{476} = 1.95$ (see above). The equilibrium value $[M/L]_{eq}$ is taken from (c) since for $\delta = 655$ μs it can be assumed that the equilibrium is largely established, and due to the measuring procedure, the data in (c) and (c′) are directly related to each other. In this way, one obtains with $[M/L]_{eq} = 2$ (from (c)), for δ(P_2,R) = 200 and 425 μs, values for τ_{rel} of 166 and 203 μs, respectively, giving a mean value $\bar{\tau}_{rel} = 185$ μs. This is much larger than the time constant of 90 μs which is obtained when the decay of L and the rise of M in Figure 2 are fitted by a single exponential.

For an understanding of this discrepancy, one has to remember the well-known fact that the rise of M can only be satisfactorily fitted by the superposition of at least two exponentials. In the present work, we found for pH 4.6 two exponentials of nearly equal amplitudes with time constants of 61 and 153 μs (see eq 4). The longer value of 153 μs is close to $\bar{\tau}_{rel} = 185$ μs. For an interpretation of this analogy, one has to realize that in our perturbation−relaxation experiment the perturbation event only starts for delay times δ(P_2,R) between 200 and 230 μs for which the initial event of M formation, described by a time constant of 61 μs, is nearly fully completed. On this basis, a model for the L−M transition at pH 4.6 is suggested which consists of two sequential L−M equilibration steps that are correlated with the fast and slow rise of M, respectively. In our perturbation−relaxation experiment, therefore, only the second step

with its longer time constant is probed. We shall come back to this model under Discussion.

L−M Equilibrium Constants for pH 4.6 and 7.3. For the L−M equilibrium which at pH 4.6 is intermediately established in the time range 300−600 μs (Figure 2), an equilibrium constant $K_{LM} \equiv k_{LM}/k_{ML} = [M]/[L]$ can be defined. For pH 7.3, besides the "fast" decay of L to M a, "slow" decay component of small amplitude was identified earlier (*28*). This may be explained by the establishment of an intermediate equilibrium also for pH 7.3, which, however, compared to pH 4.6, is considerably shifted toward M. The decay of L at pH 7.3 then may be described by a reaction sequence L ↔ M → N where the "fast" phase of the L decay refers to the establishment of an intermediate L−M equilibrium and the "slow" phase to the transition of M to N. This would imply that for pH 7.3 in the time range around $\delta = 0.5$ ms, where one expects that the equilibrium between L and M is established, the intermediate N already contributes to the L branch (Figure 2). To determine K_{LM} from the ratio [M]/[L], it is necessary to deduce the relative contributions of L and N from the composite spectra. For this purpose, in our earlier work the shift of the characteristic low-frequency band from 1539 cm^{-1} in L to 1532 cm^{-1} in N (Figure 1) was used, giving $[L]/[N] \approx 1$ for $\delta = 0.5$ ms (cf. Figure 7 of ref *28*). To check this conclusion, new experiments were carried out, whose results and analysis are summarized in Figure 7.

In the RR spectra of Figure 7, which are displayed in the region of the diagnostic bands, the contribution of the parent species is subtracted in the way described earlier (*28*). The spectra were excited at 514 nm. At this wavelength, the vibrational features of L and N dominate. Nevertheless, M can still be identified by its band at 1567 cm^{-1}. The spectra in (a) and (d) were obtained under conditions where L and N are strongly accumulated. As a basis for the analysis of the mixed spectra these spectra were simulated by a fitting procedure using Lorentzian line shapes for the individual vibrational bands. In this way the basis spectra $S_L(\tilde{\nu})$ and $S_N(\tilde{\nu})$ of "pure" L and N were obtained by superpositioning the bands l_1 and l_2 in (a) and n_1, n_2 and n_3 in (d), respectively. For convenience, the integrated RR intensities (I_L, I_N) of $S_L(\tilde{\nu})$ and $S_N(\tilde{\nu})$ were normalized to each other. The contribution of M was considered by a respective function $S_M(\tilde{\nu})$ and its integrated intensity I_M. The relative contributions of I_L, I_N, and I_M to the mixed spectra then were obtained by fitting these spectra with the sum of $S_L(\tilde{\nu})$, $S_N(\tilde{\nu})$, and $S_M(\tilde{\nu})$, respectively, and by calculating the respective relative weighting factors w_L, w_N, and w_M. These factors are given in the legend to Figure 7. In this fitting procedure, a weak band at ∼1515 cm^{-1} had still to be considered which, however, does not belong to bR or to one of its intermediates.

The relative concentrations of L and N in a mixed spectrum are given by

$$[L]/[N] = (w_L/w_N)(f_L/f_N)_{514} \quad (2)$$

where the factors f_L and f_N, as defined in eq 1, account for the different RR cross sections of the diagnostic bands in L and N for excitation at 514 nm. From particular experiments, we concluded that $(f_L/f_N)_{514} \approx 1$. This result is expected since the geometric and electronic structures of L and N are closely related to each other (*28*). In this approximation one obtains from the data in Figure 7b and with eq 2 a ratio $[L]/[N] = 1.3$ for $\delta = 0.5$ ms. In combination with the data in Figure 2, ($[L] + [N] = 0.17$ ΔBR, $[M] = 0.81$ ΔBR) one obtains K_{LM} (pH 7.3, $\delta = 0.5$ ms) = 8.4, which has to be compared with K_{LM} (pH 4.6, $\delta = 0.5$ ms) = 1.8, giving an increase in K_{LM} by a factor of 4.7 when the pH is raised from 4.6 to 7.3.

Most importantly the change of K_{LM} between pH 4.6 and 7.3 can also be directly inferred from the data in Figure 7b and e. For $\delta = 0.5$ ms one obtains

$$K_{LM}(\text{pH } 7.3)/K_{LM}(\text{pH } 4.6) = (w_M/w_L)_{\text{pH } 7.3}/(w_M/w_L)_{\text{pH } 4.6} = 4.4 \quad (3)$$

which is similar to the value obtained above.

It must be noted that for pH 7.3 a significant contribution of L is still observed for $\delta = 1$ ms giving $[L]/[N] = 0.47$ (Figure 7c). On the other hand, K_{LM} increases with δ. Thus, in analogy to eq 3, one obtains from the data in Figure 7 (b, c) an increase of K_{LM} by a factor of 1.54 between 0.5 and 1 ms. This suggests that on a longer time scale a new process sets in which favors the transition from L to M. For $\delta > 2$ ms, no residual amount of L could be identified.

Here, we briefly mention that also for pH 4.6 the L−M equilibrium is perturbed on a longer time scale. It can be seen from Figure 7 (e, f) that for $\delta \geq 0.5$ ms an increasing amount of N is formed. However, in contrast to pH 7.3, L does not disappear completely but a constant ratio between L, N, and M is formed with a time constant of 2−3 ms (data not shown) which is preserved during the recovery of BR.

The Rise of M at pH 4.6 and pH 7.2. Two transient signals, probed at 412 nm, are shown in Figure 8 which describe the rise of M at pH 4.6 and pH 7.2, respectively. These two values lie significantly below and above the pK_a of 5.6 for the release process. The transients were fitted by a sum of exponentials. For the rise of M it was necessary to use three time constants. Since on the time scale of Figure 8 the decay of M is not yet very pronounced, a single time constant (τ_d) was used. This was deduced from separate experiments on an extended time scale. For pH 4.6, one obtains $\tau_{r1} = 1.25$ μs (6%), $\tau_{r2} = 61$ μs (43%), $\tau_{r3} = 153$ μs (51%), and $\tau_d = 7.4$ ms (100%), where "r" and "d" stand for rise and decay and the numbers in parentheses give the percentages of the amplitudes. For pH 7.2, the respective values are $\tau_{r1} = 1.25$ μs (6%), $\tau_{r2} = 61$ μs (33%), $\tau_{r3} = 183$ μs (61%), and $\tau_d = 3.9$ ms (100%). The very fast rise component (1.25 μs) that appears in both transients with a small amplitude can be assigned to the rise of the L intermediate and is not further considered. The rise of M then can be described for both pH values by the superposition of a fast- and slow-rise component M_2 (τ_{r2}) and M_3 (τ_{r3}).

For an interpretation of such data, it still has to be taken into account that the amplitude of M increases by a factor of 1.41 when the pH is raised from 4.6 to 7.2 (cf. Figure 4). Thus, if the total amounts of M are set to 100 and 141 relative units (ru), one obtains for the two pH values

$$\text{pH 4.6:} \quad M_2 = 46 \text{ ru } (61\ \mu\text{s}); \quad M_3 = 54 \text{ ru } (153\ \mu\text{s})$$

$$\text{pH 7.2:} \quad M_2 = 49 \text{ ru } (61\ \mu\text{s}); \quad M_3 = 92 \text{ ru } (183\ \mu\text{s}) \quad (4)$$

The nearly identical values for M_2 indicate that the initial

rise of M is the same for both pH values. Then, as can be seen from eq 4, the increase of the total amplitude of M at pH 7.2 is due to the fact that the slow rising component M_3 is significantly larger than at pH 4.6. This behavior is also illustrated by the difference of the two transients in Figure 8, which is determined by the slow rise component. An interpretation of such effects will be given in the Discussion in terms of a model for the correlation between the L−M transition and the release process.

DISCUSSION

A Model for the L−M Transition and Its Implications. For the interpretation of the complex kinetics of the L−M transition at neutral pH, a reaction sequence of the form L ↔ M_1 → M_2 had been proposed by Váro and Lanyi (*41*) in which, in the case of wild-type bR, M_1 and M_2 are spectroscopically indistinguishable substates. Later the transition between M_1 and M_2 was correlated with the so-called "reprotonation switch" of the Schiff base, which plays a role in the various models for the proton pump mechanism (*4*). To account for the observed changes of the L−M transition below pH 7, a back reaction between M_2 and M_1 was introduced into the above sequence which was correlated with the pK_a of the proton release process (*13*). A model with sequential substates of M has recently been used by Misra et al. (*42*) for the analysis of the kinetics and pH dependence of M formation in the mutant R134K.

For the representation of our own results, we have to take into account that according to our relaxation experiment M is still directly coupled to L in the second phase of M formation. This suggests that the two phases of M formation are related to two sequential L−M equilibria with different equilibrium constants. However, for this interpretation, the problem is that no spectroscopically different states of the M or L chromophore can be identified for wild-type bR. To solve this problem, the proposal was made in a recent paper by Chizov et al. (*43*) that the change of the L−M equilibrium is controlled by the transition between two states of the protein. It is assumed that this transition changes the L−M equilibrium but not the spectroscopic states of L or M. Here we adopt this proposal, so that the time dependence of the L−M transition can be displayed in the form

$$[(\mathrm{L, Pr1}) \underset{K_1}{\overset{\tau_{r2}}{\leftrightarrow}} (\mathrm{M, Pr1})]_{\mathrm{Pr1}} \xrightarrow[\tau_{12}]{} [(\mathrm{L, Pr2}) \underset{K_2}{\overset{\tau_{r3}}{\leftrightarrow}} (\mathrm{M, Pr2})]_{\mathrm{Pr2}} \quad (5)$$

where L and M are as usually the spectroscopic states of the chromophore and Pr1 and Pr2 are different states of the environmental protein matrix. This model allows us to assign the apparent time constants that we have measured for the rise of M (eq 4) to different parts of the reaction. Thus, τ_{r2} refers to the establishment of the first L−M equilibrium (K_1), whereas τ_{r3} involves both the conversion from Pr1 to Pr2 (time constant τ_{12}) and the subsequent equilibration between L and M (K_2). Since the time constant reported for proton release lies between τ_{r2} and τ_{r3} (*8*), it is evident that the pH-dependent effects on the L−M transition, which we have ascribed to the dissociation of the release group, should be correlated with the second equilibrium in eq 5. For K_2 we have found an increase by a factor of ∼5 when the pH is raised from 4.6 to 7.3 (cf. Results).

The reaction scheme in eq 5 also allows us to explain the difference in the appearance of the two main pH-dependent effects on the L−M transition caused by the dissociation of XH. For pH >9.5, the release group is already deprotonated in the unphotolyzed state and therefore affects K_1 (acceleration of M formation) whereas for the light-induced release process (pH >5.7) it is K_2, which is influenced since the dissociation of XH is delayed with respect to the establishment of the first L−M equilibrium (K_1) (see below).

A General Scheme for the Release Process. For a discussion of the release process and the potential stages of coupling with the photocycle the following reaction sequence is proposed

$$\mathrm{XH_o} \rightarrow (\mathrm{XH})_{\mathrm{L}} \xrightarrow{k_c} (\mathrm{X-H})^*_{\mathrm{C}} \underset{k_r[\mathrm{H^+}]}{\overset{k_d}{\leftrightarrow}} \mathrm{X^-} + \mathrm{H^+(aq)} \quad (6)$$

From spectroscopic data it can be concluded that at the stage of the intermediate L, which at room temperature is formed in ∼1.25 μs (*44*), the chromophore and its protein environment with respect to the precursor K take in a new, highly ordered structure (*30*). It is likely that this conformational change of the protein induces a new intermediate state, $(XH)_L$, of the release group. It is proposed, that in the next step a reactive state, $(X-H)^*_C$ is prepared which in the subsequent phase exchanges protons with the external medium so that an intermediate dissociation equilibrium is established according to

$$k_d/k_r = K_a \equiv 10^{-pK_a}[\mathrm{M}] \quad (7)$$

Since the pK_a of the release process is ∼5.7 (*13*), the release of a proton for pH ≥7 is quasi-irreversible and since the formation of the intermediate L is fast (∼1.25 μs), the formation of $(X-H)^*_C$ is essentially determined by the rate constant k_c. The release process for pH ≥7 therefore can be approximately described by a two-step reaction sequence with rate constants k_c and k_d and the respective enthalpies of activation.

Conclusions from the Direct Detection of the Released Protons. The kinetic relationship between the L−M transition and the appearance of a proton on the extracellular surface had been first studied by Heberle and Dencher (*8*) (conditions: pH 7.5, 22 °C, 150 mM KCl). Whereas the formation of M was monitored at 412 nm, the released protons were identified by the absorbance change, $F(t)$, of the pH indicator dye fluorescein which was covalently bound to Lys-129 on the extracellular surface. The authors found that the formation of M can be fitted by the two main exponential components, for M_2 $\tau_{r2} = 44$ μs, (38%) and for M_3 $\tau_{r3} = 149$ μs (62%) (compare eq 4 and Figure 8), whereas the response function for the protonation of the dye, $F(t)$, can be described by a rise time, τ_F, of 63 μs. From the temperature dependence in the range 10−50 °C, an activation enthalpy of 64 kJ/mol was obtained for the formation of the two M components, whereas a much lower value of 35 kJ/mol was found for the protonation of the dye. An interesting observation was made by Heberle (*45*). He found that below 10 °C the values for τ_F no longer follow the linear Arrhenius plot (35 kJ/mol) but approach the values of τ_{r2} (M_2). This

implies that in the low-temperature limit the slope of the Arrhenius plot of τ_F increases and approaches the value of τ_{r2}.

Similar experiments were performed by Alexiev et al. *(9)*. They reported significant deviations from a linear Arrhenius plot of τ_F in the temperature range 5−40 °C and confirmed that in the low-temperature limit the slope of the Arrhenius plot of τ_F increases and τ_F approaches τ_{r2}. For an interpretation they suggested a two-step unidirectional reaction sequence in which the release process is triggered by the fast-rise component τ_{r2} (M_2) of the L−M transition which is followed by the ejection of the proton in a second step. At low temperatures, the L−M transition with its higher activation enthalpy (65 kJ/mol) is rate limiting for the total release process whereas at higher temperatures the subsequent reaction step, i.e., the ejection of the proton to the surface with its lower activation enthalpy, becomes rate limiting.

Linkage between the L−M Transition and Proton Release. The question is whether the release process in wild-type bR is triggered by the L−M transition. For a discussion, we consider the reaction sequences in eqs 5 and 6. According to the two-step model of Alexiev et al. (*9*), the formation of the reactive state $(X-H)_C^*$ in eq 6 would be directly correlated with the first phase of the L−M transition in eq 5 since the time constant, τ_F, for the release process lies between τ_{r2} and τ_{r3}. This would imply that k_c in eq 6 is given by $(\tau_{r2})^{-1}$. This model is consistent with the proposal that the coupling between D85 and XH, which has been inferred for the unphotolyzed state, persists in the photocycle, and therefore controls the release process (*17*, *23*).

Are our own results consistent with this proposal? We found that K_2 in eq 5 increases by a factor of ∼5 (for δ = 500 μs) when the pH is raised from 4.6 to 7.3, i.e., under conditions where the release process is completely finished. It can thus be concluded that the dissociation of XH increases the pK_a of the proton acceptor D85 by ∼0.7 pH unit if we assume that the pK_a of the Schiff base is unchanged by this process. On the other hand, a respective increase of 5 pH units was reported for the pK_a of the unphotolyzed state (*17*, *23*). This indicates that the coupling between XH and D85 is significantly weaker in the photocycle than in the parent state. It can therefore be expected that the reverse coupling, i.e., the drop of the pK_a of XH which follows on protonation of D85 in the L−M transition, is also significantly lower than the 5 pH units which were reported for the unphotolyzed state (*17*, *23*). This makes it unlikely that the decrease of the pK_a of XH from ∼9.5 in the unphotolyzed state (*17*) to 5.7 during the photocycle is exclusively due to the L−M transition. This is not surprising since the environmental conditions of D85 and XH in the photocycle are different from those in the unphotolyzed state.

From this behavior it is suggested that there may still be other mechanisms which control the release process. It must be realized that according to our present knowledge the release group appears as a molecular complex with contributions from several residues [E204 (*21*, *26*), E194 (*22*), R82 (*17*)]. It is thus conceivable that structural changes in the photocycle, for instance, during or after the formation of the intermediate L, reduce the proton affinity of this complex. In addition, it may happen that in the course of such reorientations the release complex becomes more exposed to the aqueous surface which also might reduce its proton affinity (*46*). This view suggests an alternative two-step model in which the first step, i.e., the formation of the reactive state $(X-H)_C^*$ in eq 6 is largely independent of the L−M transition. This step, which is determined by the rate constant k_c, would carry the higher of the two activation enthalpies.

In principle, values for k_c and k_d may be obtained by fitting $X^-(t,k_c k_d)$ as calculated from eq 6 to the measured response function $F(t)$. Using the data in refs *8* and *45*, one obtains $k_c \approx 33\ \mu s^{-1}$ and $k_d \approx 39\ \mu s^{-1}$ for 22 °C. Values of similar magnitude $k_c \approx 46\ \mu s^{-1}$ and $k_d \approx 51\ \mu s^{-1}$ can be inferred from the response function $F(t)$ published in ref *9*. On the other hand, k_d may be estimated from eq 7 if one assumes that k_r is diffusion controlled. Using a value $k_r = 2 \times 10^{10}\ s^{-1}\ M^{-1}$, which is typical for acids in aqueous solution (*47*), one obtains $k_d = 25\ \mu s^{-1}$. This value for k_d is by only a factor of ∼2 higher than those estimated above from the fitting procedure, indicating that the equilibration of $(X-H)_C^*$ with the aqueous medium is close to diffusion controlled. This suggests that during the photocycle the release complex becomes more exposed to the aqueous surface. If the release proton is not localized, this could also mean that the first step in eq 6 (k_c) is due to the transfer of this proton within the release complex. The "diffusion controlled" value $k_d = 25\ \mu s^{-1}$ is consistent with $k_c \approx 50\ \mu s^{-1}$ if the above described fitting procedure is applied.

The values obtained in the above-described way for k_c are close to the rate constant $(\tau_{r2})^{-1}$ for the fast-rise component M_2 (refs *8*−*10* and eq 4) so that from such data a distinction between the alternative models discussed in this section is not possible. Such a distinction also fails on the basis of kinetic deuterium effects since both the L−M transition and proton release show effects of similar magnitude (*10*, *45*).

Proton Release in Mutants of bR. Here we are interested in mutations that modify the normal release process but do not abolish it. Of great interest in this context is the mutant D85E in which the L−M transition is accelerated by more than a factor of 10, whereas the release process is delayed by a factor of ∼2 with respect to wild-type bR (*10*, *48*). The pronounced temporal delay between the two processes suggests that the L−M transition does not trigger the release function. Since the two processes do not overlap, in D_2O it can be concluded that the large kinetic deuterium effect in the release process [slowing by a factor of 4.6 (*10*)] is exclusively due to proton-transfer steps which are located within the release complex. This behavior again indicates that in D85E the release process is completely decoupled from the L−M transition.

Interesting modifications of the release process were also found for the recombinants R82Q and R82K (*17*). It turned out that in the case of R82Q the pK_a of the release group in the photocycle is only slightly decreased to 8.3 so that normal proton release is limited to pH >8.3. For R82K, the respective pK_a decreases to 6.5 and approaches the value of the wild type. This behavior suggests that the positve charge of R82 in the wild type is strongly involved in the downshift of the pK_a of the release group during the photocycle. For both mutants, the rise of M is accelerated with respect to the wild type by a factor of ∼10. This suggests that in these mutants the L−M transition does not control the release function.

CONCLUSIONS

We have shown that the time dependence of the proton transfer from the Schiff base of the bR chromophore to the counterion D85 (L−M transition) is strongly perturbed by the release of a proton from the complex XH to the aqueous surface, a process that is determined by a pK_a of 5.7. When the multiphasic L−M transition is modeled by a reaction scheme of two sequential L−M equlibria as in eq 5, it is found that proton release does not perturb the first equilibrium but shifts the second one further toward the M state. This might be interpreted in a way that the release process is triggered by the L−M transition during its first phase. This would require that the strong coupling between the pK_a values of XH and D85, which is reported for the unphotolyzed state, also holds for the photocycle. Only under such conditions the pK_a of XH in the photocycle may be reduced to a value of 5.7 once D85 becomes protonated during the L−M transition. However, we found that the shift of the L−M equilibrium as induced by proton release is much less than expected from the strong coupling between XH and D85 in the parent state, thus indicating that this coupling is significantly weaker in the photocycle. This suggests that the large reduction of the pK_a of XH to a value of 5.7 in the photocycle, and thus the release process, are not exclusively controlled by the L−M transition but are essentially caused by structural changes in which, for instance, electric charges are translocated or the release proton moves closer to the surface. This latter view is supported by our finding that the release process is close to diffusion controlled. In addition, the observation that in some mutants of bR the release process is decoupled from the fast rise of M is in line with a model in which the L−M transition is not the dominant factor that controls the release process. There is no doubt that more work will be necessary in the future to obtain a still better insight into the complexity of the proton release process in bR.

ACKNOWLEDGMENT

We thank Dr. Jürgen Troe for encouragement and support. We are indepted to our colleagues from the Max Planck Institute for Biochemistry in Munich for providing us with purple membranes. The careful preparation of the manuscript by Inge Dreger is gratefully acknowledged.

REFERENCES

1. Mathies, R. A, Lin, S. W., Ames, J. B., and Pollard, W. T. (1991) *Annu. Rev. Biophys. Biophys. Chem. 20*, 491−518.
2. Oesterhelt, D., Tittor, J., and Bamberg, E. (1992) *Bioenerget. Biomembr. 24* (2), 181−191.
3. Ebrey, T. G. (1993) in *Thermodynamics of Membranes, Receptors and Channels* (Jackson, M., Ed.) pp 353−387, CRC Press: New York.
4. Lanyi, J. K. (1993) *Biochim. Biophys. Acta 1183*, 241−261.
5. Kochendoerfer, G. G., and Mathies, R. A. (1995) *Isr. J. Chem. 35*, 211−226.
6. Braiman, M. S., Mogi, T., Marti, T., Stern, L. J., Khorana, H. G., and Rothschild, K. J. (1988) *Biochemistry 27*, 8516−8520.
7. Fahmy, K., Weidlich, O., Engelhard, M., Tittor, J., Oesterhelt, D., and Siebert, F. (1992) *Photochem. Photobiol. 56*, 1073−1083.
8. Heberle, J., and Dencher, N. A. (1992) *Proc. Natl. Acad. Sci. U.S.A. 89*, 5996−6000.
9. Alexiev, U., Mollaaghababa, R., Scherrer, P., Khorana H. G., and Heyn, M. P. (1995) *Proc. Natl. Acad. Sci. U.S.A.* 92, 372−376.
10. Cao, Y., Brown, L. S., Sasaki, J., Maeda, A., Needleman, R., and Lanyi, J. K. (1995) *Biophys. J. 68*, 1518−1530.
11. Moltke, S., Alexiev, U., and Heyn, M. P. (1995) *Isr. J. Chem. 35*, 401−414.
12. Siebert, F., Mäntele, W., and Kreutz, W. (1982) *FEBS Lett. 141* (1), 82−87.
13. Zimányi, L., Váró, G., Chang, M., Ni, B., Needleman, R., and Lanyi, J. K. (1992) *Biochemistry 31*, 8535−8543.
14. Dencher, N., and Wilms, M. (1975) *Biophys. Struct. Mech. 1*, 259−271.
15. Eisenbach M., Garty, H., Bakker, E. P., Klemperer, G., Rottenberg, H., and Caplan, S. R. (1978) *Biochemistry 17*, 4691−4698.
16. Takeuchi, Y., Ohno, K., Yoshida, M., and Nagano, K. (1981) *Photochem. Photobiol. 33*, 587−592.
17. Govindjee, R., Misra, S., Balashov, S. P., Ebrey, T. G., Crouch, R. K, and Menick, D. R. (1996) *Biophys. J. 71*, 1011−1023.
18. Scharnagl, C., Hettenkofer, J., and Fischer, S. F. (1994) *Int. J. Quantum Chem. Quantum Biol. Symp. 21*, 33−56.
19. Scharnagl, C., Hettenkofer, J., and Fischer, S. F. (1995) *Phys. Chem. 99*, 7787−7800.
20. Sampogna, R. V., and Honig, B. (1996) *Biophys. J. 71*, 1165−1171.
21. Brown, L. S., Sasaki, J., Kandori, H., Maeda, A., Needleman, and Lanyi, J. K. (1995) *J. Biol. Chem. 270*, 27122−27126.
22. Balashov, S. P., Imasheva, E. S., Ebrey, T. G., Chen, N., Menick, D. R. and Crouch, R. K. (1997) *Biochemistry 36*, 8671−8676.
23. Balashov, S. P., Imasheva, E. S., Govindjee, R., and Ebrey, T. G. (1996) *Biophys. J. 70*, 473−481.
24. Balashov, S. P., Govindjee, R., Kono, M., Imasheva, E. S., Lukashev, E., Ebrey, T. G., Crouch, R. K., Menick, D. R., and Feng, Y. (1993) *Biochemistry 32*, 10331−10343.
25. Balashov, S. P., Govindjee, R., Imasheva, E. S., Misra, S., Ebrey, T. G., Feng, Y., Crouch, R. K., and Menick, D. R. (1995) *Biochemistry 34*, 8820−8834.
26. Richter, H. T., Brown, L. S., Needleman, R., and Lanyi, J. K. (1996) *Biochemistry 35*, 4054−4062.
27. Lanyi, J. K. (1996) *Biophys. J. 71*, 541−543.
28. Eisfeld, W., Pusch, C., Diller, R., Lohrmann, R., and Stockburger, M. (1993) *Biochemistry 32*, 7196−7215.
29. Oesterhelt, D., and Stoeckenius, W. (1974) *Methods Enzymol. 31*, 667−678.
30. Althaus, T., Eisfeld, W., Lohrmann, R., and Stockburger, M. (1995) *Israel J. Chem. 35*, 227−251.
31. Hendler, R. W., Dancsházy, Z., Bose, S., Shrager, R. I., and Tokaji, Z. (1994) *Biochemistry 33*, 4604−4610.
32. Alshuth, T., and Stockburger, M. (1986) *Photochem. Photobiol. 43(1)*, 55−66.
33. Diller, R., and Stockburger, M. (1988) *Biochemistry 27*, 7641−7651.
34. Brown, L. S., Gat, Y., Sheves, M., Yamazaki, Y., Maeda, A., Needleman, R., and Lanyi, J. K. (1994) *Biochemistry 33*, 12001−12011.
35. Diller, R. (1988) Ph.D. Thesis, University of Göttingen, Göttingen, Germany.
36. Oesterhelt, D., and Hess, B. (1973) *Eur. J. Biochem. 37*, 316−326.
37. Stockburger, M., Klusmann, W., Gattermann, H., Massig, G., and Peters, R. (1979) *Biochemistry 18*, 4886−4900.
38. Ormos, P., Dancsházy, Z., and Keszthelyi, L. (1980) *Biophys. J. 31*, 207−214.
39. Butt, H. J. (1990) *Eur. Biophys. J. 19*, 31−39.
40. Althaus, T. (1996) Ph.D. Thesis, University of Göttingen, Göttingen, Germany.

41. Váro, G., and Lanyi, J. K. (1991) *Biochemistry 30*, 5008−5015.
42. Misra, S., Martin, C., Kwon, O., Ebrey, T. G., Chen, N., Crouch, R., and Menick, D. (1997) *Photochem. Photobiol. 66*, December.
43. Chizhov, I., Chernavskii, D. S., Engelhard, M., Mueller, K.-H., Zubov, B. V., and Hess, B. (1996) *Biophys. J. 71*, 2329−2345.
44. Lohrmann, R. (1992) Ph.D. Thesis, University of Göttingen, Göttingen, Germany.
45. Heberle, J. (1991) Ph.D. Thesis, University of Berlin, Berlin, Germany.
46. Honig, B., Ottolenghi, M., and Sheves, M. (1995) *Israel J. Chem. 35*, 429−446.
47. Gutman, M., and Nachliel, E. (1995) *Biochim. Biophys. Acta 1231*, 123−138.
48. Heberle, J., Oesterhelt, D., and Dencher, N. A. (1993) *EMBO J. 12(10)*, 3721−3727.

BI9714969